

# Temporal Conformal Prediction (TCP): A Distribution-Free Statistical and Machine Learning Framework for Adaptive Risk Forecasting

Agnideep Aich<sup>1\*</sup>, Ashit Baran Aich<sup>2</sup> and Dipak C. Jain<sup>3</sup>

<sup>1</sup> Department of Mathematics, University of Louisiana at Lafayette, Louisiana, USA.

<sup>2</sup> Department of Statistics, formerly of Presidency College, Kolkata, India.

<sup>3</sup> European President and Professor of Marketing, CEIBS, Shanghai, PR China.

## Abstract

We propose **Temporal Conformal Prediction (TCP)**, a distribution-free framework for constructing well-calibrated prediction intervals in nonstationary time series. TCP couples a modern quantile forecaster with a split-conformal calibration layer on a rolling window and, in its **TCP-RM** variant, augments the conformal threshold with a single online Robbins-Monro (RM) offset to steer coverage toward a target level in real time. We benchmark TCP against GARCH, Historical Simulation, a rolling tree-based Quantile Regression (QR) model, a classical linear quantile regression baseline (QR-Linear), and an adaptive conformal method (ACI) across equities (S&P 500), cryptocurrency (Bitcoin), and commodities (Gold). Three results are consistent across assets. First, both QR and QR-Linear yield the sharpest intervals but are materially under-calibrated, and even ACI remains below the nominal 95% target in our full-sample backtests. Second, TCP (and TCP-RM) achieves near-nominal coverage across assets, with intervals that are wider than Historical Simulation in this evaluation (e.g., S&P 500: 5.21 vs. 5.06). Third, the RM update changes calibration and width only marginally at our default hyperparameters. Crisis-window visualizations around March 2020 show TCP/TCP-RM expanding and then contracting their interval bands promptly as volatility spikes and recedes, with **red dots** marking days where realized returns fall outside the reported 95% interval (miscoverage). A sensitivity study confirms robustness to window size and step-size choices. Overall, TCP provides a practical, theoretically grounded solution to calibrated uncertainty quantification under distribution shift, bridging statistical inference and machine learning for risk forecasting.

**Keywords:** Temporal Conformal Prediction, Quantile Regression, Machine Learning, Statistical Learning, Value-at-Risk, Financial Time Series, Risk Management.

*MSC 2020 Subject Classification:* 62G08, 62M10, 62P05, 91G70, 68T05

## 1. INTRODUCTION

Financial risk estimation is more than a regulatory checkbox; it is foundational for market stability and investor confidence [Markowitz, 1952, J.P. Morgan/Reuters, 1996]. Yet, when markets enter turbulent regimes, traditional risk models often fall short. Early implementations

---

\*Corresponding author: Agnideep Aich, [agnideep.aich1@louisiana.edu](mailto:agnideep.aich1@louisiana.edu), ORCID: [0000-0003-4432-1140](https://orcid.org/0000-0003-4432-1140)

of Value-at-Risk (VaR) were predominantly parametric, often assuming (conditional) normality [Jorion, 2007, Dowd, 1998], assumptions that can systematically understate tail risk. Coherent alternatives such as Conditional Value-at-Risk (CVaR) were introduced to address some of these limitations [Rockafellar and Uryasev, 2000]. Events like the 2008 global financial crisis [Brunnermeier, 2009] and the March 2020 stock-market crash [Mazur et al., 2021] exposed the fragility of parametric assumptions, especially in the tails.

The core challenge is that financial returns violate the independent and identically distributed (i.i.d.) assumption that underpins many statistical learning techniques. Real-world returns are heteroskedastic, exhibit regime shifts, and often exhibit heavy tails [Cont, 2001]. GARCH-type models [Engle, 1982, Bollerslev, 1986] can capture some volatility clustering, but they still depend on pre-specified distributions and lack reliable coverage guarantees for interval forecasts.

In recent years, conformal prediction has gained traction as a powerful distribution-free framework for quantifying uncertainty. Classical conformal methods provide finite-sample coverage guarantees without assuming a particular data distribution [Vovk et al., 2005]. However, these guarantees rest on exchangeability, a condition often violated by time series with temporal dependencies. Several works extend conformal methods to sequential or temporally dependent settings [Xu and Xie, 2021, Stankeviciute et al., 2021, Gibbs and Candès, 2021], but a robust and practical solution for financial markets remains an open challenge.

This paper closes that gap. We introduce **Temporal Conformal Prediction (TCP)**, a real-time, adaptive framework for constructing well-calibrated prediction intervals for financial time series. TCP combines a modern machine-learning quantile forecaster with an online conformal calibration layer governed by a modified Robbins–Monro scheme. Crucially, this architecture bridges statistical inference and machine learning, combining the theoretical rigor of conformal methods with the flexibility of a data-driven approach that can adapt to non-stationarity, volatility clustering, and abrupt market shifts.

We benchmark TCP across three major asset classes, **equities (S&P 500)**, **cryptocurrency (Bitcoin)**, and **commodities (Gold)**, against established models like GARCH, Historical Simulation, a tree-based Quantile Regression (QR) forecaster, a classical linear quantile regression baseline (QR-Linear), and an adaptive conformal method (ACI). Our results highlight a critical flaw in static ML approaches: both QR and QR-Linear produce sharp intervals but are systematically under-calibrated, and ACI improves calibration only partially. By contrast, TCP demonstrates superior adaptive capabilities, adjusting its intervals in response to market volatility so that empirical coverage stays close to the 95% target. This adaptive property, which we visualize during the March 2020 crash, makes TCP a more reliable and principled framework for real-world risk management. A comprehensive sensitivity analysis further underscores the robustness of our framework to key hyperparameters.

We organize the paper as follows. Section 2 surveys related work. Section 3 establishes our mathematical notation. Section 4 lays out the TCP theory. Section 5 details our empirical setup, including model architectures and the evaluation framework. Section 6 presents our main findings, including benchmark comparisons, visualizations, and hyperparameter sensitivity analysis. Finally, Section 7 offers practical takeaways and future directions.

## 2. RELATED WORK

Before detailing our proposed TCP framework, we situate our work within the existing literature. We review three areas that inform our approach: traditional financial risk models, the

evolution of time-series forecasting with machine learning, and the theoretical foundations of conformal prediction.

**Traditional Financial Risk Models.** Quantitative risk management traces its roots to portfolio theory [Markowitz, 1952] and was formalized around the VaR concept with J.P. Morgan’s RiskMetrics [J.P. Morgan/Reuters, 1996]. In practice, three VaR paradigms have dominated: parametric approaches (often assuming conditional normality), non-parametric Historical Simulation, and Monte Carlo methods [Jorion, 2007, Dowd, 1998, Glasserman, 2004]. Beyond VaR, CVaR provided a coherent alternative for tail-risk control [Rockafellar and Uryasev, 2000]. However, many traditional approaches underperform in crisis backtests [Kupiec, 1995, Christoffersen, 1998], highlighting a blind spot when tail events dominate.

**Advanced Time-Series and Machine-Learning Models.** To better capture time-varying variance and volatility clustering, the GARCH family became foundational [Engle, 1982, Bollerslev, 1986]; asymmetric variants such as EGARCH and GJR-GARCH address leverage and sign effects [Nelson, 1991, Glosten et al., 1993]. For heavy-tailed markets, extreme value theory (EVT) offers principled tail modeling [III, 1975, McNeil and Frey, 2000], and VaR under heavy tails raises specific concerns [Danielsson and de Vries, 2000]. On the machine-learning side, quantile regression directly targets conditional quantiles [Koenker and Bassett, 1978], with ensemble and neural variants such as quantile regression forests [Meinshausen, 2006] and quantile networks [Taylor, 2000]; deep LSTMs capture complex temporal dependencies [Fischer and Krauss, 2018]. We also emphasize the computational efficiency of gradient-boosted trees via LightGBM for quantile forecasting [Ke et al., 2017].

**Conformal Prediction Theory.** Conformal prediction provides distribution-free, finite-sample prediction sets under exchangeability [Vovk et al., 2005]. Recent advances relax these assumptions for sequential or non-stationary settings through adaptive calibration and time-series-aware procedures [Gibbs and Candès, 2021, Xu and Xie, 2021, Stankeviciute et al., 2021]. Our work builds on these foundations with a practical adaptive conformal framework tailored to financial risk forecasting, combining local split-conformal calibration with an online Robbins–Monro offset for temporal adaptation.

**Adaptive and Time-Series Conformal Prediction.** Recent research has addressed non-stationary environments by adapting the conformal guarantee. Gibbs and Candès [2021] and Zaffran et al. [2022] introduce Adaptive Conformal Inference (ACI), which updates the target miscoverage rate ( $\alpha_t$ ) online based on past coverage errors. While effective, we argue that in heavy-tailed financial settings, oscillating the target probability can lead to unstable interval widths; TCP-RM instead adapts the conformal threshold ( $C_t$ ) directly via a Robbins-Monro update, offering a stable, scalar lever for width control. Other approaches, such as CPTD [Lin et al., 2022], leverage cross-sectional exchangeability across a panel of time series to restore validity. In contrast, TCP is designed for the univariate setting (single asset) where cross-sectional pooling (e.g., mixing Bitcoin and Gold) is inappropriate due to distinct, idiosyncratic asset dynamics.

### 3. NOTATION

Having reviewed the relevant literature, we now establish the mathematical notation that will be used throughout the remainder of the paper. A clear notational framework is essential for formally developing our proposed method in the subsequent sections.

We denote the price of a financial asset at time  $t$  as  $P_t$ , and its corresponding daily log-return

as  $r_t$ . The primary objective is to construct a  $(1 - \alpha)$  prediction interval, denoted by  $[\ell_{t+1}, u_{t+1}]$ , for the next return  $r_{t+1}$ , where  $\alpha \in (0, 1)$  is the specified miscoverage rate. The feature space for our models includes lagged returns and realized volatility  $\sigma_t$ .

**Learning and Prediction:** For a general learning problem with  $n$  observations, we consider feature-label pairs as  $(X_i, Y_i)$  and a generic point prediction model as  $\hat{f}(\cdot)$ . Our time series evaluation runs for  $T$  total time steps. We use  $\mathcal{F}_t$  to represent the filtration (information set) available up to time  $t$ . The true, unknown  $\tau$ -quantile of the return distribution is  $q_\tau$ . Our quantile regression model,  $\mathcal{F}_\tau$ , produces a data-driven estimate of this quantile, denoted  $\hat{q}_\tau$ .

**Conformal Prediction (two-sided, split).** At each time  $t$  we use a rolling window of size  $w$  split into a training slice  $\mathcal{T}_t$  and a calibration slice  $\mathcal{C}_t$  with  $|\mathcal{T}_t| + |\mathcal{C}_t| = w$ . Quantile forecasters  $\hat{q}_{\alpha/2}$  and  $\hat{q}_{1-\alpha/2}$  are fit on  $\mathcal{T}_t$  only (no leakage). Two-sided nonconformity scores on the calibration slice are

$$s_i = \max\{\hat{q}_{\alpha/2}(X_i) - r_i, r_i - \hat{q}_{1-\alpha/2}(X_i), 0\}, \quad i \in \mathcal{C}_t.$$

Let  $m = |\mathcal{C}_t|$  and  $s_{(1)} \leq \dots \leq s_{(m)}$  be the order statistics. We set the conformal threshold  $C_t = s_{(k)}$  with  $k = \lceil (m + 1)(1 - \alpha) \rceil$ , and the next-step interval  $[\ell_{t+1}, u_{t+1}] = [\hat{q}_{\alpha/2}(X_{t+1}) - C_t, \hat{q}_{1-\alpha/2}(X_{t+1}) + C_t]$ . For comparability, the QR baseline is evaluated in the same walk-forward fashion using only the training slice  $|\mathcal{T}_t|=w_{\text{tr}}$  (no calibration slice), i.e., it is rolling and out-of-sample.

**Adaptive Calibration:** The online adaptive calibration is driven by the coverage error at time  $t$ , defined as  $e_t = \mathbb{1}(r_t \notin [\ell_t, u_t]) - \alpha$ . The threshold is updated using a learning rate  $\gamma_t$ , which is itself controlled by hyperparameters  $\gamma_0, \lambda$ , and  $\beta$ .

**Benchmark Models:** For the benchmark models, we denote the conditional variance from the GARCH model as  $\hat{\sigma}_t^2$ , which is governed by parameters  $\omega, \alpha_{\text{GARCH}}$ , and  $\beta_{\text{GARCH}}$ . For Historical Simulation, we use  $\bar{r}$  to represent the mean return over a rolling window.

**Mathematical Operators:** Finally, we use standard mathematical operators, including  $\Pr(\cdot)$  for probability,  $\mathbb{E}[\cdot]$  for expectation,  $\mathbf{1}(\cdot)$  for the indicator function,  $\text{sign}(\cdot)$  for the sign function, and  $\lfloor \cdot \rfloor$  for the floor function.

**Variants used (terminology).** We consider two closely related procedures. **TCP** applies split-conformal prediction on a rolling window, and **TCP-RM** augments TCP with a Robbins-Monro offset applied to the conformal threshold based on past coverage errors. Formal definitions and update equations are given in Section 4.4.

## 4. MATHEMATICAL BACKGROUND

This section lays the theoretical groundwork for our proposed method. Our calibration mechanism is related in spirit to adaptive conformal procedures for nonstationary settings [Zaffran et al., 2022, Lin et al., 2022] but differs in using a Robbins-Monro update on the conformal threshold while holding the nominal level fixed. We begin by formally defining the problem of prediction interval forecasting, then review the principles of classical conformal prediction and its limitations, and finally develop the core mathematical components of our Temporal Conformal Prediction (TCP) framework and its adaptive calibration mechanism.

### 4.1 Problem Formulation

We begin by framing the central task of this paper. We consider a univariate financial time series of daily log-returns  $\{r_1, r_2, \dots, r_t\}$ , where  $r_t = \log(P_t/P_{t-1})$  and  $P_t$  is the asset price

at time  $t$ . Our objective is to construct a prediction interval  $[\ell_{t+1}, u_{t+1}]$  for the next return  $r_{t+1}$  that satisfies the nominal coverage property  $\Pr(r_{t+1} \in [\ell_{t+1}, u_{t+1}]) \approx 1 - \alpha$  for a given miscoverage level  $\alpha \in (0, 1)$ . Traditional methods often fail to achieve this in the presence of non-stationarity, motivating our distribution-free approach.

## 4.2 Classical Conformal Prediction

To motivate our approach, we first briefly review the classical conformal prediction framework, which provides strong guarantees but relies on an assumption that is often violated in our target domain.

Given a set of i.i.d. observations  $\{(X_i, Y_i)\}_{i=1}^n$  from an unknown distribution, conformal prediction provides a framework for generating prediction sets with finite-sample coverage guarantees. This is achieved through a non-conformity score.

**Definition 4.1 (Non-Conformity Score)** *A mapping  $A((X_i, Y_i)) \mapsto \alpha_i \in \mathbb{R}$  that quantifies how poorly a data point  $(X_i, Y_i)$  conforms to a given model or dataset. A higher score implies a poorer fit.*

For a new test point  $X_{n+1}$ , the prediction set  $\Gamma_{1-\alpha}(X_{n+1})$  is formed by all possible values  $y$  whose non-conformity score  $A(X_{n+1}, y)$  is less than or equal to the  $(1 - \alpha)$ -quantile of the scores from the training set. Formally, if we define the empirical p-value for a candidate value  $y$  as  $p(y) = \frac{1}{n+1} \sum_{i=1}^{n+1} \mathbf{1}(\alpha_i \geq A(X_{n+1}, y))$ , the prediction set is:

$$\Gamma_{1-\alpha}(X_{n+1}) = \{y : p(y) > \alpha\}.$$

**Theorem 4.1 (Finite-Sample Validity)** *If the sequence of pairs  $\{(X_i, Y_i)\}_{i=1}^{n+1}$  is exchangeable, then the conformal prediction set  $\Gamma_{1-\alpha}$  satisfies:*

$$\Pr(Y_{n+1} \in \Gamma_{1-\alpha}(X_{n+1})) \geq 1 - \alpha.$$

A common choice for the non-conformity score is the absolute residual,  $\alpha_i = |Y_i - \hat{f}(X_i)|$ , where  $\hat{f}$  is a point prediction model.

A full proof is provided in Appendix A.

## 4.3 Temporal Conformal Prediction (TCP)

The exchangeability assumption required by classical conformal prediction is too restrictive for financial time series. Here, we build upon its principles to develop our TCP method, which relaxes this assumption to hold only within a local time window. Our proposed TCP method, outlined in Algorithm 1, leverages this principle.

## 4.4 Adaptive Calibration (TCP vs. TCP-RM)

We consider two variants. **TCP** is split-conformal only: at each time  $t$ , the window  $\mathcal{W}_t$  of size  $w$  is split into a training slice  $\mathcal{T}_t$  and a calibration slice  $\mathcal{C}_t$  with  $|\mathcal{T}_t| + |\mathcal{C}_t| = w$ . Quantile forecasters  $\hat{q}_{\alpha/2}, \hat{q}_{1-\alpha/2}$  are fit on  $\mathcal{T}_t$  and the two-sided nonconformity scores on  $\mathcal{C}_t$  yield the split-conformal threshold  $C_t = s_{(k)}$ ,  $k = \lceil (|\mathcal{C}_t| + 1)(1 - \alpha) \rceil$ . **TCP-RM** augments TCP with a single online

**Algorithm 1** Temporal Conformal Prediction (TCP) at time  $t$  (split-conformal, two-sided)

**Require:** Returns  $\{r_1, \dots, r_t\}$ ; features  $\{X_1, \dots, X_t\}$ ; window  $w$  with  $w_{\text{tr}} + w_{\text{cal}} = w$ ; miscoverage  $\alpha \in (0, 1)$

1: **Define slices:**  $\mathcal{W}_t = \{t-w+1, \dots, t\}$ ;  $\mathcal{T}_t = \{t-w+1, \dots, t-w_{\text{cal}}\}$ ;  $\mathcal{C}_t = \{t-w_{\text{cal}}+1, \dots, t\}$

2: **Fit forecasters on  $\mathcal{T}_t$ :** train  $\hat{q}_{\alpha/2}, \hat{q}_{1-\alpha/2}$  on  $\{(X_i, r_i) : i \in \mathcal{T}_t\}$

3: **Compute two-sided nonconformity on  $\mathcal{C}_t$ :**

4: **for each  $i \in \mathcal{C}_t$  do**

5:  $s_i \leftarrow \max\{\hat{q}_{\alpha/2}(X_i) - r_i, r_i - \hat{q}_{1-\alpha/2}(X_i), 0\}$

6:  $m \leftarrow |\mathcal{C}_t|$ ; sort  $s_{(1)} \leq \dots \leq s_{(m)}$

7: **Conformal threshold:**  $k \leftarrow \lceil (m+1)(1-\alpha) \rceil$ ;  $C_t \leftarrow s_{(k)}$

8: **Form next-step interval:**

9:  $\ell_{t+1} \leftarrow \hat{q}_{\alpha/2}(X_{t+1}) - C_t$ ;  $u_{t+1} \leftarrow \hat{q}_{1-\alpha/2}(X_{t+1}) + C_t$

**Ensure:** Prediction interval  $[\ell_{t+1}, u_{t+1}]$

offset  $C_t^{\text{RM}}$  updated by Robbins–Monro:

$$C_{t+1}^{\text{RM}} = C_t^{\text{RM}} + \gamma_t (\mathbf{1}\{r_t \notin [\ell_t, u_t]\} - \alpha), \quad (1)$$

$$\gamma_t = \frac{\gamma_0}{(1 + \lambda t)^\beta}, \quad \beta \in (1/2, 1]. \quad (2)$$

The effective threshold is  $C_t^{\text{eff}} = C_t + C_t^{\text{RM}}$ , giving  $[\ell_{t+1}, u_{t+1}] = [\hat{q}_{\alpha/2}(X_{t+1}) - C_t^{\text{eff}}, \hat{q}_{1-\alpha/2}(X_{t+1}) + C_t^{\text{eff}}]$ . No manual decay or heuristic shrinkage is used.

**Assumptions.** (A1) (*Bounded scores*)  $\{s_i\}$  are a.s. bounded. (A2) (*Local mixing*) The process is  $\beta$ -mixing so that  $e_t - \mathbb{E}[e_t | \mathcal{F}_{t-1}]$  is a martingale-difference with bounded variance. (A3) (*Monotone coverage in  $C$* )  $g(C) = \Pr(r_t \in [\ell_t, u_t] | C)$  is continuous and strictly increasing near the unique  $C^*$  with  $g(C^*) = 1 - \alpha$ . (A4) (*Stepsizes*)  $\gamma_t > 0$ ,  $\sum_t \gamma_t = \infty$ ,  $\sum_t \gamma_t^2 < \infty$ .

Under (A1)–(A4), TCP provides local finite-sample validity on  $\mathcal{C}_t$ ; TCP-RM adds asymptotic calibration in time via (1).

**Clarifications on Assumptions (A1–A4).** To make the role of the assumptions explicit in the analysis and in Theorem 4.2, we record the following clarifications:

1. **Stochastic approximation framework.** The Robbins–Monro update for the offset is analyzed using classical stochastic-approximation arguments under mixing and bounded-variance noise; our assumptions instantiate those conditions in this setting ([Kushner and Yin, 2003]).
2. **TCP-RM guarantees.** Under (A1)–(A4), the time-average coverage converges to the target level and the effective threshold converges to a fixed point (Theorem 4.2).
3. **TCP baseline (split-conformal).** TCP uses split-conformal calibration within a rolling window; this is a local working approximation to exchangeability, and we do not claim global finite-sample validity for the full time series.
4. **Assumption verification in practice.** We empirically probe the mixing/independence assumptions using standard risk diagnostics (Kupiec [1995] and Christoffersen [1998] backtests); the lack of serial dependence in exceedances supports the validity of these conditions on our financial datasets.

## 4.5 Proof of Asymptotic Calibration

**Theorem 4.2** *Under the Robbins–Monro update (1) and (A1)–(A4),  $\frac{1}{T} \sum_{t=1}^T \mathbf{1}\{r_t \in [\ell_t, u_t]\} \rightarrow 1 - \alpha$  a.s., and  $C_t \rightarrow C^*$  a.s.*

Full proof is given in Appendix A.

**Remark 4.1 (Practical stability)** *To enforce (A1) and keep the iterates bounded, we only enforce nonnegativity of the effective threshold by projecting the RM offset:*

$$C_{t+1}^{\text{RM}} \leftarrow \max \left\{ C_t^{\text{RM}} + \gamma_t (\mathbf{1}\{r_t \notin [\ell_t, u_t]\} - \alpha), -C_t \right\},$$

so that  $C_{t+1}^{\text{eff}} = C_t + C_{t+1}^{\text{RM}} \geq 0$ . An additional upper cap  $S_t$  (e.g., a high empirical quantile of the calibration scores  $s_i$ ) can be included, but we did not use it in our experiments. This projection is standard in stochastic approximation and does not change the prediction rule.

## 5. METHODOLOGY

With the theoretical foundations of TCP established in the previous section, we now turn to our empirical study. This section details the methodology used to evaluate TCP’s performance, including the data and features, the specific model implementations, and the evaluation framework.

### 5.1 Data and Feature Construction

The foundation of any forecasting model is the data it learns from. We begin by describing the financial assets used in our analysis and the construction of the feature set designed to capture relevant market dynamics.

We analyze daily log-returns,  $r_t = \log(P_t/P_{t-1})$ , for three distinct asset classes: **Equities** (S&P 500), **Cryptocurrencies** (Bitcoin), and **Commodities** (Gold), using data from November 2017 to May 2025. For each asset, we construct a feature set for our models based on recent historical data. The features include:

- **Lagged Returns:**  $\{r_{t-k}\}_{k=1}^5$  to capture short-term momentum and autoregressive effects.
- **Rolling Volatility:**

$$\sigma_t = \sqrt{\frac{1}{20-1} \sum_{k=1}^{20} (r_{t-k} - \bar{r}_{t,20})^2}, \quad (3)$$

$$\bar{r}_{t,20} = \frac{1}{20} \sum_{k=1}^{20} r_{t-k}. \quad (4)$$

Here  $\sigma_t$  is the rolling *sample* standard deviation of the past 20 returns, computed with denominator 20 – 1 (in pandas this corresponds to `.rolling(20).std(ddof=1)`).

- **Nonlinear Transformations:** The squared prior return,  $r_{t-1}^2$ , and its sign,  $\text{sign}(r_{t-1})$ , to account for non-linear dependencies and leverage effects.

## 5.2 Forecasting Models

To fairly assess the contribution of our proposed method, we benchmark it against several established alternatives. Here, we describe the implementation of TCP and the three competing models: Quantile Regression, GARCH, and Historical Simulation.

### 5.2.1 Temporal Conformal Prediction (TCP)

Our proposed model first estimates the conditional quantiles,  $\hat{q}_\tau(t)$ , using a gradient-boosted tree model,  $\mathcal{F}_\tau$ , trained on the feature set described above. The prediction interval is formed from the forecaster’s two quantiles and the split-conformal threshold  $C_t$  computed on a disjoint calibration slice (Alg. 1). In the TCP-RM variant,  $C_t$  is further updated online via (1). This threshold is updated at each time step based on the observed coverage error, as detailed in Section 4. The entire process is performed sequentially on a rolling basis with a window of  $w = 252$  days.

### 5.2.2 Benchmark Models

1. **Quantile Regression (QR):** Same gradient-boosted quantile forecaster as TCP, evaluated sequentially in a rolling, out-of-sample manner on a trailing window of  $w_{\text{tr}}=192$  observations (no conformal calibration).
2. **Linear Quantile Regression (QR-Linear):** Classical *linear* quantile regression trained with the pinball loss at  $\alpha/2$  and  $1 - \alpha/2$ , using the same features and the same rolling, out-of-sample protocol as QR (window  $w_{\text{tr}}=192$ ; no calibration slice). This baseline is included in the full-sample numerical benchmarks (Table 1), but we omit it from the crisis-window visualizations to avoid clutter; its behavior is intermediate between QR and ACI.
3. **Adaptive Conformal Inference (ACI):** A rolling implementation of [Gibbs and Candès \[2021\]](#) that uses the same window split as TCP ( $w_{\text{tr}} = 192$  training,  $w_{\text{cal}} = 60$  calibration). However, instead of updating the conformal threshold  $C_t$  (like TCP-RM), ACI updates the target miscoverage rate  $\alpha_t$  online based on the most recent coverage error (step size  $\eta = 0.05$ ).
4. **Fixed-parameter GARCH(1,1) (EWMA):** Conditional variance updated recursively

$$\sigma_t^2 = \omega + \alpha r_{t-1}^2 + \beta \sigma_{t-1}^2, \quad (5)$$

$$(\omega, \alpha, \beta) = (10^{-6}, 0.05, 0.9), \quad (6)$$

with coefficients held fixed and updated sequentially using only past data (no rolling re-estimation). One-step-ahead  $(1 - \alpha)$  intervals assume conditional normality with zero mean, i.e.,  $[-z_{1-\alpha/2}\sigma_t, z_{1-\alpha/2}\sigma_t]$ .

5. **Historical Simulation (Hist):** Non-parametric empirical  $(\alpha/2, 1 - \alpha/2)$  quantiles from a rolling 252-day window.

## 5.3 Evaluation Framework

To provide a rigorous comparison, we define clear success criteria for all models. Our primary metrics are (i) marginal empirical coverage of the prediction intervals and (ii) average interval

width (sharpness). In addition, we apply standard VaR backtests on the 5% lower tail implied by the 95% two-sided intervals.

We use two core summary metrics:

- **Empirical Coverage:** The proportion of out-of-sample observations that fall within their respective prediction intervals,  $\frac{1}{T} \sum_{t=1}^T \mathbf{1}\{r_t \in [\ell_t, u_t]\}$ . The primary goal is to match the nominal coverage rate of  $1 - \alpha = 95\%$ .
- **Average Interval Width (Sharpness):** The average width of the prediction intervals,  $\frac{1}{T} \sum_{t=1}^T (u_t - \ell_t)$ . Sharper (narrower) intervals are preferred, provided that the target coverage is met.

**VaR-style backtests.** For each model and asset, we also perform standard 1-day-ahead VaR backtests on the 5% lower tail. Specifically, we report: (i) the unconditional coverage test of Kupiec [1995] ( $\text{LR}_{\text{uc}}$ ), (ii) the independence test of Christoffersen [1998] ( $\text{LR}_{\text{ind}}$ ), and (iii) their sum  $\text{LR}_{\text{cc}} = \text{LR}_{\text{uc}} + \text{LR}_{\text{ind}}$  for conditional coverage. Each test yields a likelihood-ratio statistic and a  $p$ -value, together with the number of exceedances  $x$  (days where the realized return falls below the nominal 5% VaR) out of  $n$  out-of-sample predictions.

Our empirical analysis therefore evaluates models along two dimensions, i.e., global calibration–sharpness, via empirical coverage and average width over the full sample, and risk-management diagnostics in the left tail, via the Kupiec/Christoffersen backtests.

## 6. RESULTS AND DISCUSSION

We now assess **Temporal Conformal Prediction (TCP)** and our main contribution **TCP-RM** (TCP with a Robbins–Monro online calibration layer) against a set of baselines (ACI, QR, QR-Linear, GARCH, Historical Simulation) on three asset classes: *S&P 500*, *BTC-USD*, and *Gold*. The goal is to test whether the online calibration delivers near-nominal coverage under distribution shift while preserving sharpness.

Evaluation centers on two criteria: (i) empirical coverage versus the nominal target  $1 - \alpha = 0.95$ , and (ii) average interval width as a measure of sharpness. Table 1 summarizes full-sample performance; Figure 1 visualizes behavior during the COVID-19 crash. We also report a hyperparameter sensitivity study (window size  $w$ , stepsize  $\gamma_0$ ) to assess robustness of TCP-RM. QR-Linear appears in the full-sample benchmark table but is omitted from the crisis-window plots and window-level summary tables to keep the figures legible; numerically, its coverage and width lie between QR and ACI.

### Main Findings: Adaptiveness and Calibration

Three findings emerge from Table 1 and the crisis-window visualization (Fig. 1):

(i) **Calibration vs. sharpness trade-off across learning baselines.** The rolling ML baselines (QR, QR-Linear, ACI) yield substantially narrower intervals than TCP/TCP-RM, but remain under-calibrated relative to the 95% target, which is consistent with the VaR backtests where only TCP and TCP-RM are not rejected. Among these baselines, QR-Linear and ACI partially improve calibration over tree-based QR at the price of somewhat wider bands, yet all three still fall short of nominal coverage.

(ii) **TCP/TCP-RM achieve near-nominal coverage with wider bands than Historical Simulation.** TCP coverage is close to the 95% target on all assets (SP500 95.2%,

Table 1: Model Performance Across Assets (Target Coverage: 95%)

Asset	Model	Empirical Coverage	Avg. Interval Width	Predictions
SP500	TCP	0.9523	5.2097	1448
	TCP-RM	0.9530	5.2171	1448
	ACI	0.8736	3.7894	1448
	QR	0.8322	3.3106	1508
	QR-Linear	0.8846	4.2746	1508
	GARCH	0.8269	3.0505	1670
	Hist	0.9312	5.0575	1468
BTC-USD	TCP	0.9537	20.8879	1448
	TCP-RM	0.9537	20.8859	1448
	ACI	0.8874	16.3529	1448
	QR	0.8554	12.6764	1508
	QR-Linear	0.8952	17.4916	1508
	GARCH	0.8533	11.3908	1670
	Hist	0.9441	18.0576	1468
Gold	TCP	0.9427	4.7368	1448
	TCP-RM	0.9427	4.7438	1448
	ACI	0.8294	2.9901	1448
	QR	0.8302	2.8249	1508
	QR-Linear	0.8932	3.9780	1508
	GARCH	0.8365	2.6185	1670
	Hist	0.9326	4.0238	1468

BTC-USD 95.4%, Gold 94.3%). Relative to Historical Simulation, TCP/TCP-RM intervals are systematically wider (SP500: 5.21 vs. 5.06; BTC-USD: 20.89 vs. 18.06; Gold: 4.74 vs. 4.02), reflecting stricter calibration under elevated volatility. Historical Simulation attains high but slightly sub-nominal coverage (93–94%) with narrower bands, consistent with its reliance on a long empirical window that smooths abrupt regime changes.

**(iii) Robbins–Monro adds negligible change at these hyperparameters.** TCP–RM’s coverage and width are essentially identical to TCP across assets (coverage deltas  $\leq 0.0007$ ; width deltas  $\leq 0.01$ ), indicating that the additional Robbins–Monro offset has minimal incremental effect at the chosen  $(w, \gamma_0)$  settings.

GARCH under-covers consistently (about 82–85% coverage) while being sharper than the calibrated methods, consistent with its conditional-Gaussian specification being slow to adapt to asymmetric tails during stress.

**Crisis-window coverage.** To stress-test the models, we also examine a 55-day “COVID crisis” window from February–April 2020 for each series. For this sub-period we compute the empirical coverage and average width of the 95% prediction intervals. Table 2 reports the results for the S&P 500; the corresponding tables for BTC-USD and Gold are given in Appendix B.

For the S&P 500, TCP and TCP–RM both achieve 80% coverage with very similar average widths (11.94 and 11.95, respectively). GARCH attains the same coverage (80%) with a narrower interval (average width 9.66), while the rolling quantile regression and historical bench-

Table 2: Crisis-window empirical coverage and average width of 95% prediction intervals for the S&P 500 during the COVID shock (Feb–Apr 2020,  $n = 55$  days).

Model	Coverage	Avg. width	$n$
TCP	0.8000	11.9371	55
TCP-RM	0.8000	11.9511	55
QR (rolling)	0.6545	9.1315	55
GARCH	0.8000	9.6571	55
Hist	0.6545	5.9058	55
ACI	0.5636	4.6307	55

mark produce even sharper intervals (average widths 9.13 and 5.91) at the cost of substantially lower coverage (65.45% each). ACI is the most aggressive, with the narrowest intervals (average width 4.63) but only 56.36% coverage. Thus, during the sharpest part of the COVID shock, all methods under-cover, but TCP and TCP-RM remain competitive with GARCH in terms of the calibration-sharpness trade-off, while clearly dominating ACI and the nonparametric baselines in coverage.

**TCP versus TCP–RM.** Figure 2 overlays TCP and TCP–RM intervals with the realized returns during the COVID window for the S&P 500; analogous plots for BTC-USD and Gold are provided in Appendix C. The bands for TCP and TCP–RM are almost indistinguishable in all three series, and this is confirmed quantitatively.

Over the COVID window, TCP and TCP–RM have identical empirical coverage for each asset (0.8000 for S&P 500, 0.8909 for BTC-USD, and 0.8727 for Gold), and their average interval widths differ only at the third decimal place: 11.94 vs 11.95 for S&P 500, 24.28 vs 24.27 for BTC-USD, and 6.81 vs 6.81 for Gold. Over the full sample, the two methods also remain nearly identical: for S&P 500, coverage is 0.9523 for TCP and 0.9530 for TCP–RM with average widths 5.2097 vs 5.2171 and interval scores 7.1168 vs 7.1157; for BTC-USD, both methods achieve coverage 0.9537 with widths 20.8879 vs 20.8859 and interval scores 27.9846 vs 27.9851; for Gold, both achieve coverage 0.9427 with widths 4.7368 vs 4.7438 and interval scores 6.3246 vs 6.3246. In other words, the Robbins–Monro adaptation layer leaves the marginal predictive performance of TCP essentially unchanged while preserving its good calibration properties.

*Implementation note (comparability).* All learning-based methods (TCP, TCP-RM, ACI, QR, QR-Linear) use the same feature set. TCP/TCP-RM and ACI are evaluated out-of-sample with a rolling window of 252 points split into 192 training and 60 calibration points. Rolling QR and QR-Linear are also evaluated out-of-sample using a 192-point trailing training window without a separate calibration slice. The differences in the “Predictions” counts (e.g., 1508 for QR/QR-Linear vs. 1448 for TCP/TCP-RM/ACI, 1468 for Hist, 1670 for GARCH) reflect these distinct warm-up requirements. Aligning the evaluation horizon to the longest warm-up yields qualitatively identical conclusions: tree-based QR remains sharp but under-calibrated; QR-Linear and ACI partially trade width for better coverage yet stay sub-nominal; and TCP/TCP-RM are near-nominal and, in this evaluation, wider than Historical Simulation.

## 6.1 Backtests of tail coverage

To complement marginal coverage and interval width, we perform standard VaR-style backtests on the 5% lower tail using the Kupiec [Kupiec, 1995] unconditional coverage test (LR\_uc), the

Christoffersen [Christoffersen, 1998] independence test (LR\_ind), and their joint conditional coverage test (LR\_cc). Table 3 reports the likelihood-ratio statistics,  $p$ -values, the total number of exceedances (days where the realized return falls below the nominal 5% lower bound), and the number of out-of-sample predictions  $n$  for the S&P 500.

Table 3: VaR-style backtests on the 5% lower tail for S&P 500.

Model	LR_uc	p_uc	LR_ind	p_ind	LR_cc	p_cc	Exceed.	$n$
TCP	0.170625	0.679557	2.022260	0.155008	2.192885	0.334057	69	1448
TCP-RM	0.287050	0.592117	2.203339	0.137712	2.490389	0.287885	68	1448
ACI	127.325197	0	7.171877	0.007406	134.497073	0	183	1448
QR	280.342540	0	1.404329	0.236000	281.746869	0	253	1508
QR-Linear	100.761827	0	10.714099	0.001063	111.475925	0	174	1508
GARCH	334.481845	0	0.022234	0.881466	334.504079	0	289	1670
Hist	9.827570	0.001719	22.904448	0.000002	32.732018	0	101	1468

On S&P 500, TCP and TCP-RM are the only methods that pass all three backtests at conventional significance levels: their LR\_uc, LR\_ind, and LR\_cc  $p$ -values stay well above 0.05, and the number of exceedances (68–69) is close to the 5% target ( $\approx 0.05 \times 1448$ ). By contrast, ACI, QR, QR-Linear, GARCH, and Historical Simulation are all strongly rejected by at least one of the tests: their LR\_uc and LR\_cc statistics are very large with  $p$ -values numerically equal to zero (e.g., QR: 253 exceedances; GARCH: 289; Hist: 101). This confirms that, on equities, only TCP/TCP-RM deliver statistically acceptable 95% tail coverage. The corresponding backtests for BTC-USD and Gold show the same qualitative pattern and are reported in Appendix D.

We also perform sensitivity analyses for TCP-RM and TCP, with results reported in Appendix F and Appendix G. TCP vs. TCP-RM trace plots are presented in Appendix H.

## 7. CONCLUSION AND FUTURE WORK

This paper introduced **Temporal Conformal Prediction (TCP)**, a simple framework for calibrated prediction intervals in nonstationary time series. TCP combines a rolling, exchangeability-aware split-conformal layer with a modern quantile forecaster, while the **TCP-RM** variant adds a single Robbins–Monro offset that adjusts the conformal threshold online using observed coverage errors.

Across three asset classes, TCP and TCP-RM achieve a strong calibration–sharpness balance: coverage stays close to the 95% target and the intervals are wider than Historical Simulation, reflecting stricter calibration in volatile periods. The rolling tree-based QR model and the classical linear baseline (QR-Linear) produce the narrowest bands but undershoot the target coverage, especially in turbulent regimes, and the adaptive conformal baseline (ACI) only partially corrects this undercoverage. In our study, TCP and TCP-RM are the only methods that simultaneously passes standard VaR backtests and maintains competitive sharpness on S&P 500, BTC-USD, and Gold.

Like any sequential method, TCP can temporarily under-cover during abrupt regime shifts before calibration catches up. Performance depends on the quality of the base quantile forecaster and the windowing scheme, and very heavy tails or structural breaks can stress any fixed feature set. In our experiments, TCP-RM leaves average calibration and sharpness essentially unchanged at the chosen hyperparameters, but its Robbins–Monro layer provides a principled online mechanism that can correct coverage drift when step sizes are tuned more aggressively;

overly aggressive step sizes can, however, overcorrect. On the positive side, TCP provides distribution-free, time-adaptive intervals that align naturally with backtesting and governance needs in risk management, and its single-threshold, model-agnostic design makes deployment straightforward in production pipelines.

Several extensions follow naturally. On the modeling side, it is natural to develop multivariate and portfolio versions of TCP, target conditional or localized coverage (for example by volatility state), explore richer quantile forecasters and feature sets, design change-point-aware adaptations that shorten transients after regime breaks, and study heavy-tail robustness through EVT-inspired or asymmetric nonconformity scores. On the application side, TCP intervals can be mapped directly to VaR/ES, margin, and capital rules and evaluated in realistic backtests for utility and capital efficiency. Beyond finance, the same adaptive, distribution-free mechanism could support calibrated uncertainty in domains such as biostatistics and medicine (for example ICU vitals or glucose-range forecasting), epidemiology, genetics and genomics, sports analytics, renewable energy, and operations or transportation planning wherever nonstationarity and reliable uncertainty quantification are central.

In sum, TCP offers a compact, distribution-free, and adaptive route to calibrated uncertainty quantification under temporal drift. Its empirical performance, visual adaptiveness in crisis windows, and robustness to sensible hyperparameters suggest that it is a practical default for risk forecasting and a promising building block for broader sequential decision systems.

## References

- Tim Bollerslev. Generalized autoregressive conditional heteroskedasticity. *Journal of Econometrics*, 31(3):307–327, 1986.
- Markus K. Brunnermeier. Deciphering the liquidity and credit crunch 2007–2008. *Journal of Economic Perspectives*, 23(1):77–100, 2009.
- Peter F. Christoffersen. Evaluating interval forecasts. *International Economic Review*, 39(4):841–862, 1998.
- Rama Cont. Empirical properties of asset returns: Stylized facts and statistical issues. *Quantitative Finance*, 1(2):223–236, 2001.
- Jon Danielsson and Casper G. de Vries. Value-at-risk and extreme returns. *Annals of Economics and Statistics*, 60:239–270, 2000.
- Kevin Dowd. *Beyond Value-at-Risk: The New Science of Risk Management*. John Wiley & Sons, Chichester, UK, 1998.
- Robert F. Engle. Autoregressive conditional heteroskedasticity with estimates of the variance of united kingdom inflation. *Econometrica*, 50(4):987–1007, 1982.
- Thomas Fischer and Christopher Krauss. Deep learning with long short-term memory networks for financial market predictions. *European Journal of Operational Research*, 270(2):654–669, 2018.
- Isaac Gibbs and Emmanuel Candès. Adaptive conformal inference under distribution shift. In *Advances in Neural Information Processing Systems*, pages 1660–1672, 2021.
- Paul Glasserman. *Monte Carlo Methods in Financial Engineering*. Springer, New York, 2004.

- Lawrence R. Glosten, Ravi Jagannathan, and David E. Runkle. On the relation between the expected value and the volatility of the nominal excess return on stocks. *Journal of Finance*, 48(5):1779–1801, 1993.
- James Pickands III. Statistical inference using extreme order statistics. *Annals of Statistics*, 3(1):119–131, 1975.
- Philippe Jorion. *Value-at-Risk: The New Benchmark for Managing Financial Risk*. McGraw-Hill, New York, 3 edition, 2007.
- J.P. Morgan/Reuters. Riskmetrics technical document. Technical report, 1996.
- Guolin Ke, Qi Meng, Thomas Finley, Taifeng Wang, Wei Chen, Weidong Ma, Qiwei Ye, and Tie-Yan Liu. LightGBM: A highly efficient gradient boosting decision tree. In *Advances in Neural Information Processing Systems*, pages 3146–3154, 2017.
- Roger Koenker and Gilbert Bassett. Regression quantiles. *Econometrica*, 46(1):33–50, 1978.
- Paul H. Kupiec. Techniques for verifying the accuracy of risk measurement models. *The Journal of Derivatives*, 3(2):73–84, 1995.
- Harold J. Kushner and G. George Yin. *Stochastic Approximation and Recursive Algorithms and Applications*. Springer-Verlag, New York, 2 edition, 2003.
- Zhen Lin, Ting Cai, and Lei Wang. Conformal prediction intervals with temporal dependence. *Transactions on Machine Learning Research*, 2022. ISSN 2835-8856.
- Harry Markowitz. Portfolio selection. *Journal of Finance*, 7(1):77–91, 1952.
- Mieszko Mazur, Mykola Dang, and Miguel Vega. Covid-19 and the march 2020 stock market crash: Evidence from s&p 1500. *Finance Research Letters*, 38:101690, 2021.
- Alexander J. McNeil and Rüdiger Frey. Estimation of tail-related risk measures for heteroscedastic financial time series: An extreme value approach. *Journal of Empirical Finance*, 7(3–4):271–300, 2000.
- Nicolai Meinshausen. Quantile regression forests. *Journal of Machine Learning Research*, 7: 983–999, 2006.
- Daniel B. Nelson. Conditional heteroskedasticity in asset returns: A new approach. *Econometrica*, 59(2):347–370, 1991.
- R. Tyrrell Rockafellar and Stanislav Uryasev. Optimization of conditional value-at-risk. *Journal of Risk*, 2(3):21–41, 2000.
- Kamile Stankeviciute, Ahmed M. Alaa, and Mihaela van der Schaar. Conformal time-series forecasting. In *Advances in Neural Information Processing Systems*, pages 6216–6228, 2021.
- James W. Taylor. A quantile regression neural network approach to estimating the conditional density of multiperiod returns. *Journal of Forecasting*, 19(4):299–311, 2000.
- Vladimir Vovk, Alexander Gammerman, and Glenn Shafer. *Algorithmic Learning in a Random World*. Springer, New York, 2005.

Chen Xu and Yao Xie. Conformal prediction interval for dynamic time-series forecasting. In *Proceedings of the 38th International Conference on Machine Learning*, pages 11559–11569, 2021.

Margaux Zaffran, Aymeric Dieuleveut, Yannig Goude, Julie Josse, and Stefano Ermon. Adaptive conformal predictions for time series. In *Proceedings of the 39th International Conference on Machine Learning*, volume 162 of *Proceedings of Machine Learning Research*, pages 25834–25866. PMLR, 2022.

## Code Availability

Full code is available at <https://github.com/agnivibes/temporal-conformal-prediction-tcp>.

## A. MATHEMATICAL PROOFS

This section provides the proofs of Theorems 4.1 and 4.2.

### A.1 Proof of Finite-Sample Validity (Theorem 4.1)

**Theorem Statement.** Under exchangeability of the pairs  $\{(X_i, Y_i)\}_{i=1}^{n+1}$ , the conformal prediction set  $\Gamma_{1-\alpha}$  satisfies:

$$\Pr(Y_{n+1} \in \Gamma_{1-\alpha}(X_{n+1})) \geq 1 - \alpha.$$

**Proof.** Let the set of non-conformity scores be  $\mathcal{A} = \{\alpha_1, \dots, \alpha_n, \alpha_{n+1}\}$ , where  $\alpha_i = A(X_i, Y_i)$  for  $i = 1, \dots, n+1$ . The core assumption of exchangeability implies that any permutation of the sequence of pairs  $(X_1, Y_1), \dots, (X_{n+1}, Y_{n+1})$  is equally likely. Consequently, any permutation of the scores in  $\mathcal{A}$  is also equally likely.

This symmetry implies that the rank of the test score  $\alpha_{n+1}$  within the set  $\mathcal{A}$  is uniformly distributed on  $\{1, 2, \dots, n+1\}$ . Let us define the rank of  $\alpha_{n+1}$  as  $R_{n+1} = \sum_{i=1}^{n+1} \mathbf{1}(\alpha_i \leq \alpha_{n+1})$ . Due to exchangeability, we have  $\Pr(R_{n+1} = k) = \frac{1}{n+1}$  for any  $k \in \{1, \dots, n+1\}$ .

The conformal prediction set is defined as  $\Gamma_{1-\alpha}(X_{n+1}) = \{y : p(y) > \alpha\}$ , where the p-value  $p(y)$  is the fraction of scores greater than or equal to the score of the candidate point  $(X_{n+1}, y)$ . The true observation  $Y_{n+1}$  is excluded from this set if and only if its p-value is less than or equal to  $\alpha$ . The p-value for the true observation is  $p(Y_{n+1}) = \frac{1}{n+1} \sum_{i=1}^{n+1} \mathbf{1}(\alpha_i \geq \alpha_{n+1})$ .

The event of miscoverage,  $Y_{n+1} \notin \Gamma_{1-\alpha}(X_{n+1})$ , occurs if  $p(Y_{n+1}) \leq \alpha$ . This is equivalent to the rank of  $\alpha_{n+1}$  being “small.” Specifically,  $\frac{R_{n+1}}{n+1} \leq \alpha$ , which implies  $R_{n+1} \leq \lfloor \alpha(n+1) \rfloor$ .

We can now bound the probability of this miscoverage event:

$$\Pr(Y_{n+1} \notin \Gamma_{1-\alpha}(X_{n+1})) = \Pr(R_{n+1} \leq \lfloor \alpha(n+1) \rfloor) = \sum_{k=1}^{\lfloor \alpha(n+1) \rfloor} \Pr(R_{n+1} = k).$$

Since  $\Pr(R_{n+1} = k) = \frac{1}{n+1}$ , this sum is:

$$\sum_{k=1}^{\lfloor \alpha(n+1) \rfloor} \frac{1}{n+1} = \frac{\lfloor \alpha(n+1) \rfloor}{n+1} \leq \frac{\alpha(n+1)}{n+1} = \alpha.$$

Therefore, the probability of miscoverage is at most  $\alpha$ , which implies that the probability of correct coverage is at least  $1 - \alpha$ . This completes the proof. ■

## A.2 Proof of Asymptotic Calibration (Theorem 4.2)

**Theorem.** Under (A1)–(A4) and the update  $C_{t+1} = C_t + \gamma_t e_t$  with  $e_t = \mathbf{1}\{r_t \notin [\ell_t, u_t]\} - \alpha$ , we have  $C_t \rightarrow C^*$  a.s. where  $g(C^*) = 1 - \alpha$ , and  $\frac{1}{T} \sum_{t=1}^T \mathbf{1}\{r_t \in [\ell_t, u_t]\} \rightarrow 1 - \alpha$  a.s.

**Proof. Step 1 (Notation and stability).** Let  $\mathcal{F}_t$  be the filtration generated by the data up to time  $t$ . Define  $g(C) = \Pr(r_t \in [\ell_t, u_t] \mid C_t = C)$  and  $\phi(C) = \mathbb{E}[e_t \mid C_t = C] = \alpha - g(C)$ . By (A3),  $\phi$  is continuous and strictly decreasing in a neighborhood of its unique root  $C^*$  with  $\phi(C^*) = 0$ . Under (A1) the two-sided nonconformity scores are bounded, hence there exists  $S < \infty$  such that valid thresholds lie in  $[0, S]$ . Without loss of generality we assume the recursion is kept in a compact interval (e.g., via projection onto  $[0, S]$ ); this is standard in SA and does not change the produced intervals.

**Step 2 (SA decomposition).** Decompose the coverage error into signal + noise:

$$e_t = \mathbb{E}[e_t \mid \mathcal{F}_{t-1}] + \Delta_t = \phi(C_t) + \Delta_t,$$

where  $\Delta_t := e_t - \mathbb{E}[e_t \mid \mathcal{F}_{t-1}]$  is a martingale-difference sequence with  $\mathbb{E}[\Delta_t \mid \mathcal{F}_{t-1}] = 0$  and uniformly bounded second moments by (A2). The recursion becomes

$$C_{t+1} = C_t + \gamma_t \{\phi(C_t) + \Delta_t\}. \quad (7)$$

**Step 3 (Convergence of  $C_t$  to  $C^*$ ).** Consider the Lyapunov function  $V(c) = (c - C^*)^2$ . From (7),

$$C_{t+1} - C^* = (C_t - C^*) + \gamma_t \{\phi(C_t) + \Delta_t\},$$

hence

$$V(C_{t+1}) = (C_t - C^*)^2 + 2\gamma_t(C_t - C^*)\{\phi(C_t) + \Delta_t\} + \gamma_t^2\{\phi(C_t) + \Delta_t\}^2.$$

Taking conditional expectation and using  $\mathbb{E}[\Delta_t \mid \mathcal{F}_{t-1}] = 0$ ,

$$\mathbb{E}[V(C_{t+1}) \mid \mathcal{F}_{t-1}] = V(C_t) + 2\gamma_t(C_t - C^*)\phi(C_t) + \gamma_t^2 \mathbb{E}[\{\phi(C_t) + \Delta_t\}^2 \mid \mathcal{F}_{t-1}].$$

By (A1)–(A2) and compactness of the state space, there exists  $K < \infty$  with  $\mathbb{E}[(\phi(C_t) + \Delta_t)^2 \mid \mathcal{F}_{t-1}] \leq K$  a.s. By (A3),  $\phi$  is strictly decreasing near  $C^*$ , hence there exists  $\eta > 0$  and  $\rho > 0$  such that  $(C - C^*)\phi(C) \leq -\eta(C - C^*)^2$  whenever  $|C - C^*| \leq \rho$ . Since iterates remain in a compact interval and step-sizes decrease, standard SA stability (together with projection if used) ensures that eventually  $|C_t - C^*| \leq \rho$  a.s. (alternatively, one may argue by contradiction using the drift term). Therefore, for all large  $t$ ,

$$\mathbb{E}[V(C_{t+1}) \mid \mathcal{F}_{t-1}] \leq V(C_t) - 2\eta\gamma_t(C_t - C^*)^2 + K\gamma_t^2.$$

By the Robbins–Siegmund supermartingale convergence lemma, since  $\sum_t \gamma_t^2 < \infty$  and  $V(\cdot) \geq 0$ , we obtain that  $V(C_t)$  converges a.s. and  $\sum_t \gamma_t(C_t - C^*)^2 < \infty$  a.s. Because  $\sum_t \gamma_t = \infty$  (A4), the latter implies  $\liminf_t (C_t - C^*)^2 = 0$ , and together with the monotone drift near  $C^*$  yields  $C_t \rightarrow C^*$  almost surely.

**Step 4 (Time-average calibration).** Recall  $e_t = \phi(C_t) + \Delta_t$ . Since  $C_t \rightarrow C^*$  and  $\phi$  is continuous,  $\phi(C_t) \rightarrow 0$  a.s.; by Cesàro averaging,  $\frac{1}{T} \sum_{t=1}^T \phi(C_t) \rightarrow 0$  a.s. By (A2) and square-integrability of  $\Delta_t$ , the strong law for martingale differences (e.g., Hall & Heyde, 1980) implies  $\frac{1}{T} \sum_{t=1}^T \Delta_t \rightarrow 0$  a.s. Hence

$$\frac{1}{T} \sum_{t=1}^T e_t = \frac{1}{T} \sum_{t=1}^T \phi(C_t) + \frac{1}{T} \sum_{t=1}^T \Delta_t \xrightarrow{\text{a.s.}} 0.$$

Equivalently,  $\frac{1}{T} \sum_{t=1}^T \mathbf{1}\{r_t \in [\ell_t, u_t]\} \rightarrow 1 - \alpha$  a.s., which completes the proof. ■

## B. ADDITIONAL CRISIS-WINDOW RESULTS

Table 4 and Table 5 report the COVID crisis-window coverage and widths for BTC-USD and Gold.

Table 4: Crisis-window empirical coverage and average width of 95% prediction intervals for BTC-USD during COVID (Feb–Apr 2020,  $n = 55$  days).

Model	Coverage	Avg. width	$n$
TCP	0.8909	24.2814	55
TCP-RM	0.8909	24.2729	55
QR (rolling)	0.8909	17.4407	55
GARCH	0.8545	17.9290	55
Hist	0.9091	19.8499	55
ACI	0.8727	20.2050	55

Table 5: Crisis-window empirical coverage and average width of 95% prediction intervals for Gold during COVID (Feb–Apr 2020,  $n = 55$  days).

Model	Coverage	Avg. width	$n$
TCP	0.8727	6.8087	55
TCP-RM	0.8727	6.8119	55
QR (rolling)	0.7455	4.0744	55
GARCH	0.8000	4.9112	55
Hist	0.6909	3.9957	55
ACI	0.5818	2.6643	55

## C. ADDITIONAL TCP VS TCP-RM CRISIS-WINDOW PLOTS

Figure 3 and Figure 4 show the TCP and TCP-RM 95% prediction intervals alongside returns for BTC-USD and Gold during the COVID crisis window (Feb–Apr 2020).

## D. ADDITIONAL BACKTESTS

Table 6 reports the same Kupiec and Christoffersen 5% lower-tail backtests for BTC-USD and Gold. The qualitative pattern matches the S&P 500 results in the main text: TCP and TCP-RM are the only models that are not rejected by any of the three tests on either asset, while ACI, QR, QR-Linear, GARCH, and Historical Simulation accumulate far too many exceptions and fail at least one of the diagnostics.

Table 6: VaR-style backtests on the 5% lower tail for BTC-USD and Gold.

Asset	Model	LR_uc	p_uc	LR_ind	p_ind	LR_cc	p_cc	Exceed.	$n$
BTC-USD	TCP	0.434337	0.509868	1.094155	0.295552	1.528492	0.465685	67	1448
	TCP-RM	0.434337	0.509868	1.094155	0.295552	1.528492	0.465685	67	1448
	ACI	89.465919	0	11.093370	0.000866	100.559289	0	163	1448
	QR	192.386083	0	0.868073	0.351489	193.254155	0	218	1508
	QR-Linear	73.429698	0	5.932611	0.014863	79.362309	0	158	1508
	GARCH	221.469896	0	1.342326	0.246624	222.812222	0	245	1670
	Hist	1.023574	0.311673	9.776309	0.001768	10.799882	0.004517	82	1468
Gold	TCP	1.563187	0.211199	0.338333	0.560793	1.901519	0.386447	83	1448
	TCP-RM	1.563187	0.211199	0.338333	0.560793	1.901519	0.386447	83	1448
	ACI	280.191360	0	2.694226	0.100712	282.885586	0	247	1448
	QR	288.442776	0	1.452719	0.228092	289.895494	0	256	1508
	QR-Linear	78.288019	0	13.470197	0.000242	91.758217	0	161	1508
	GARCH	291.399454	0	1.952267	0.162343	293.351721	0	273	1670
	Hist	8.513620	0.003525	2.757010	0.096829	11.270630	0.003570	99	1468

## E. ADDITIONAL VISUALIZATIONS OF THE PREDICTION INTERVALS

This section provides the prediction interval visualizations for BTC-USD (5) and Gold (6) during the COVID-19 market crash (February-April 2020).

## F. SENSITIVITY ANALYSIS FOR TCP-RM

This section reports the full hyperparameter sensitivity analysis for **TCP-RM** across the S&P 500, BTC-USD, and Gold. For each asset we vary the rolling window size  $w \in \{100, 252, 500\}$  and the initial Robbins-Monro step size  $\gamma_0 \in \{0.005, 0.01, 0.05\}$  while keeping the calibration slice fixed at  $|\mathcal{C}| = 40$ . For every configuration, we report empirical coverage of the nominal 95% prediction intervals and average interval width (Tables 7, 8, and 9).

Table 7: TCP-RM sensitivity on S&P 500 with  $|\mathcal{C}| = 40$  (target 95%).

Hyperparameters		Performance	
Window Size ( $w$ )	$\gamma_0$	Coverage	Interval Width
100	0.005	0.9575	5.3052
100	0.010	0.9575	5.3066
100	0.050	0.9581	5.3172
252	0.005	0.9579	5.1168
252	0.010	0.9579	5.1191
252	0.050	0.9586	5.1314
500	0.005	0.9525	5.4135
500	0.010	0.9525	5.4319
500	0.050	0.9567	5.5348

*Summary.* On S&P 500,  $w=252$  yields the narrowest intervals (width  $\approx 5.12$ ), with  $w=100$  and  $w=500$  producing slightly wider bands and coverage close to or just above the 95% tar-

Table 8: TCP-RM sensitivity on **BTC-USD** with  $|\mathcal{C}| = 40$ .

Hyperparameters		Performance	
Window Size ( $w$ )	$\gamma_0$	Coverage	Interval Width
100	0.005	0.9575	21.7806
100	0.010	0.9575	21.7819
100	0.050	0.9575	21.7926
252	0.005	0.9572	21.6138
252	0.010	0.9572	21.6154
252	0.050	0.9572	21.6285
500	0.005	0.9608	20.5050
500	0.010	0.9608	20.5053
500	0.050	0.9608	20.5071

Table 9: TCP-RM sensitivity on **Gold** with  $|\mathcal{C}| = 40$ .

Hyperparameters		Performance	
Window Size ( $w$ )	$\gamma_0$	Coverage	Interval Width
100	0.005	0.9494	4.6437
100	0.010	0.9494	4.6460
100	0.050	0.9494	4.6643
252	0.005	0.9461	4.7812
252	0.010	0.9461	4.7868
252	0.050	0.9468	4.8285
500	0.005	0.9500	5.1058
500	0.010	0.9500	5.1188
500	0.050	0.9542	5.2031

get, except for mild undercoverage in some  $w=500$  settings; this motivates our choice  $w=252$ ,  $\gamma_0=0.01$  in the main experiments. For BTC-USD, interval widths shrink as  $w$  increases, with the tightest bands at  $w=500$ , while coverage remains stably around 95–96% across all configurations. For Gold, widths are smallest at  $w=100$  and grow with  $w$ , and coverage stays near the nominal level throughout. Across all three assets, TCP-RM is therefore stable over the  $(w, \gamma_0)$  grid considered here: the window length  $w$  controls the sharpness–stability tradeoff, whereas the specific choice of  $\gamma_0$  within this range has only a minor effect on coverage and width.

## G. SENSITIVITY ANALYSIS ON TCP (NO RM)

For completeness, in Tables 10, 11 and 12, we also report sensitivity for **TCP** (split-conformal only, no Robbins–Monro offset). We vary  $w \in \{100, 252, 500\}$  with  $|\mathcal{C}| = 40$  for each asset.

As with TCP-RM, the effect of  $w$  is asset-dependent (e.g., BTC narrows as  $w$  increases; SP500 is tightest near  $w=252$ ; Gold widens with larger  $w$ ). Without the adaptive offset, coverage can dip slightly below 95% in some settings, underscoring the benefit of the online calibration layer.

Table 10: TCP sensitivity on **S&P 500** with  $|\mathcal{C}| = 40$ .

Window Size ( $w$ )	Coverage	Interval Width
100	0.9575	5.3038
252	0.9572	5.1145
500	0.9508	5.3951

Table 11: TCP sensitivity on **BTC-USD** with  $|\mathcal{C}| = 40$ .

Window Size ( $w$ )	Coverage	Interval Width
100	0.9575	21.7792
252	0.9572	21.6121
500	0.9608	20.5048

## H. TCP VS. TCP-RM TRACE PLOTS

This section provides TCP and TCP-RM trace plots for all three assets (Figures 7, 8 and 9). Each panel shows daily returns, the corresponding 95% prediction intervals, a rolling coverage diagnostic, and the evolution of the conformal thresholds.

Table 12: TCP sensitivity on **Gold** with  $|\mathcal{C}| = 40$ .

Window Size ( $w$ )	Coverage	Interval Width
100	0.9487	4.6414
252	0.9454	4.7756
500	0.9492	5.0928

SP500: Model Intervals During COVID-19 Crash (Feb-Apr 2020)

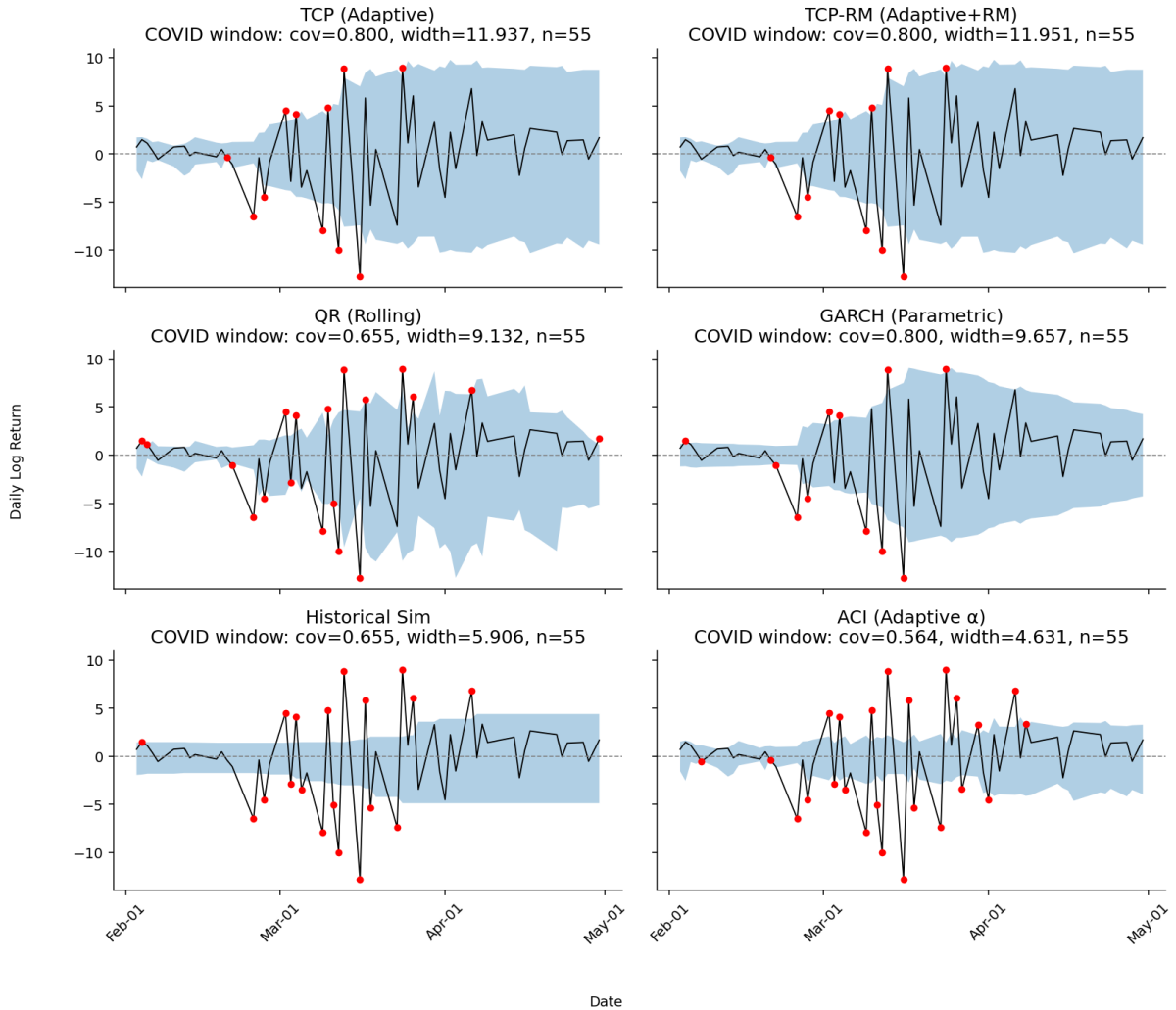


Figure 1: A comparison of 95% prediction intervals from **six** models (TCP, TCP-RM, QR, GARCH, Hist, ACI) for S&P 500 daily returns during the COVID-19 market crash (Feb-Apr 2020). Shaded bands show the interval; the **red dots** mark days where the realized return falls outside the 95% interval (miscoverage). TCP/TCP-RM bands widen rapidly into the March spike and contract in April, while ACI maintains relatively narrow bands and under-covers more frequently. Analogous crisis-window panels for BTC-USD and Gold appear in Appendix E.

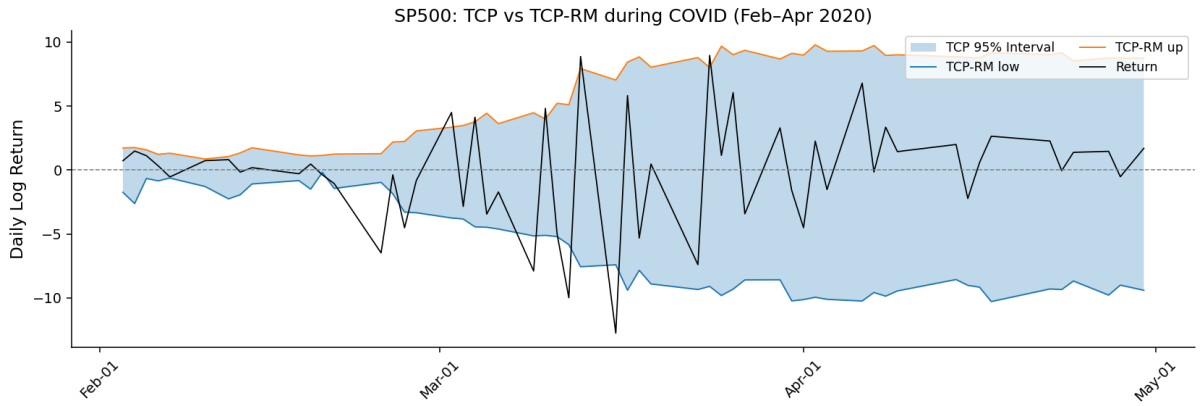


Figure 2: S&P 500: TCP vs TCP-RM 95% prediction intervals during the COVID crisis window (Feb-Apr 2020).

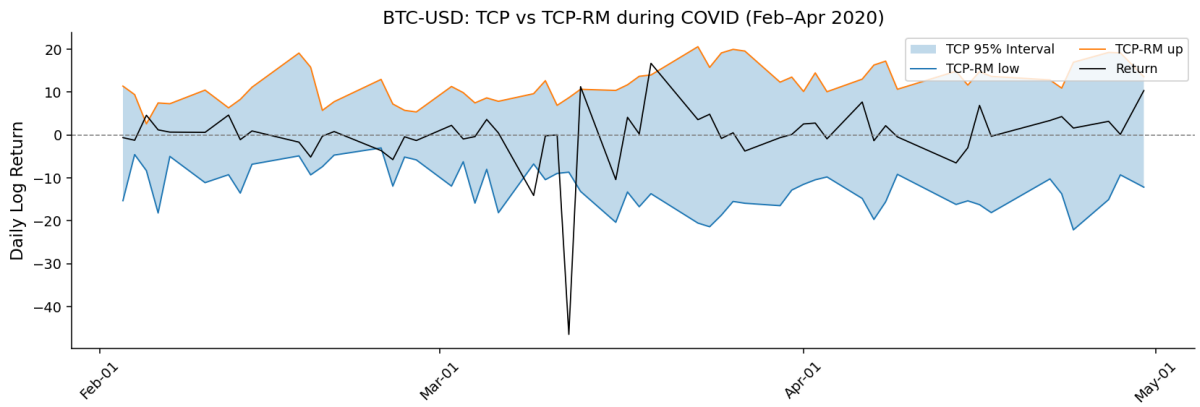


Figure 3: BTC-USD: TCP vs TCP-RM 95% prediction intervals during the COVID crisis window (Feb-Apr 2020).

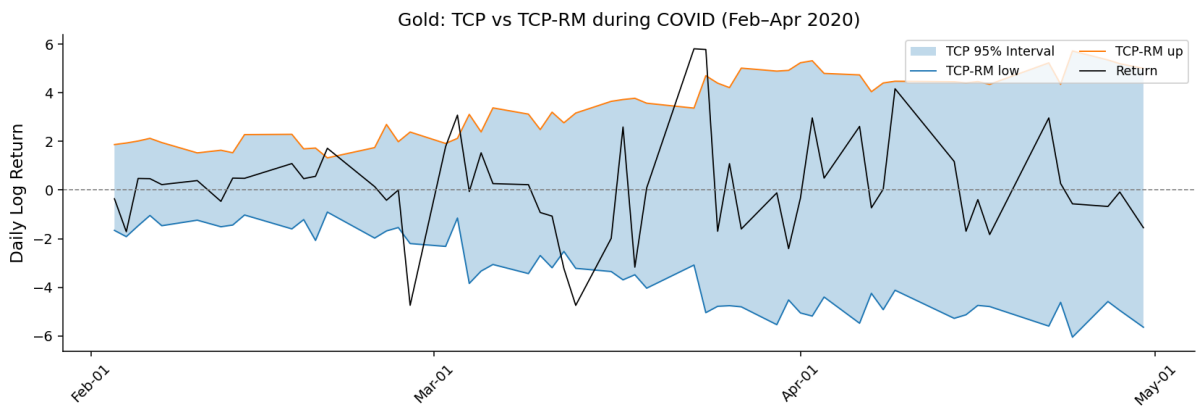


Figure 4: Gold: TCP vs TCP-RM 95% prediction intervals during the COVID crisis window (Feb-Apr 2020).

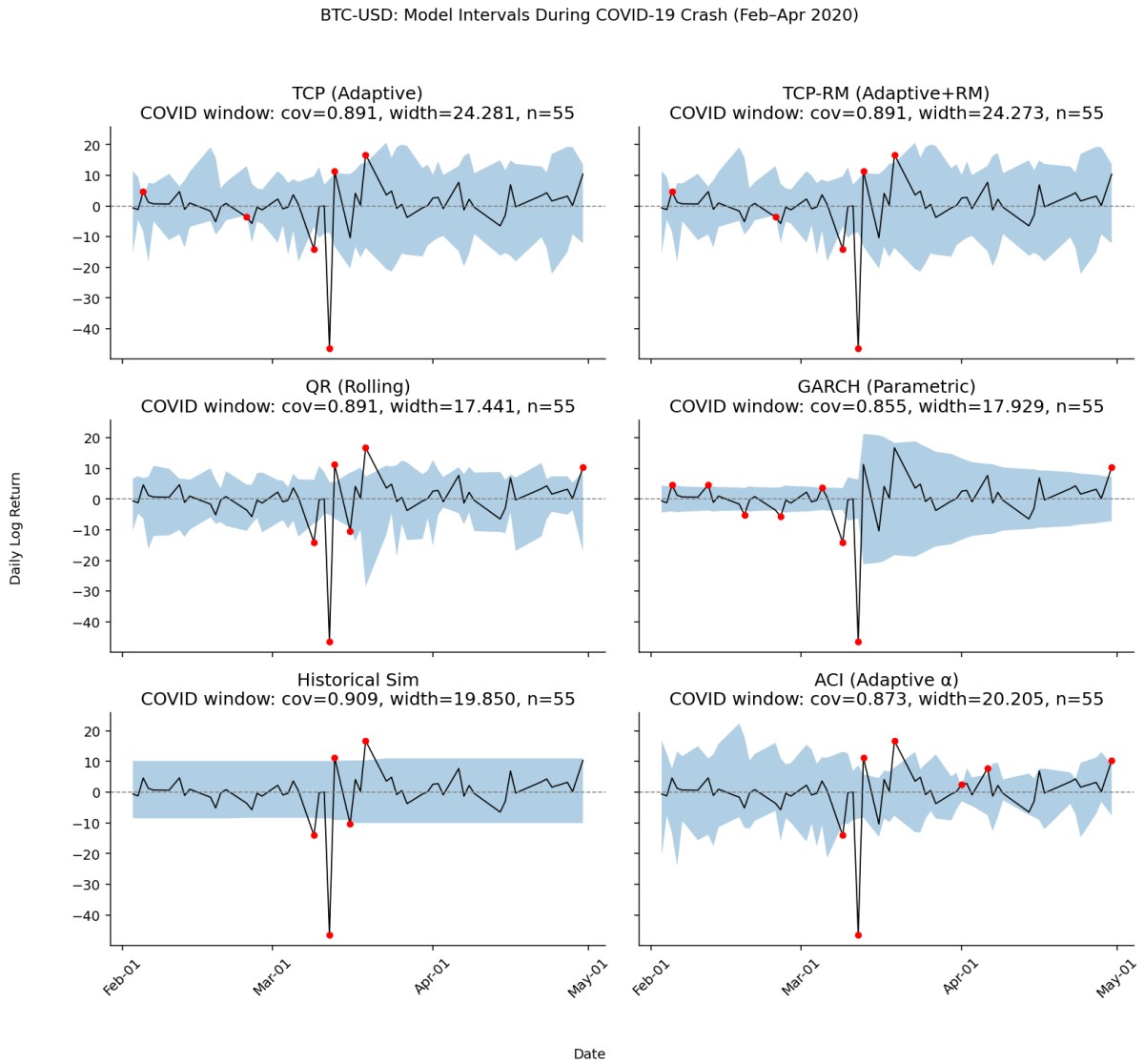


Figure 5: A comparison of 95% prediction intervals from **five** models (TCP, TCP-RM, QR, GARCH, Hist, ACI) for BTC-USD daily returns during the COVID-19 market crash (February-April 2020).

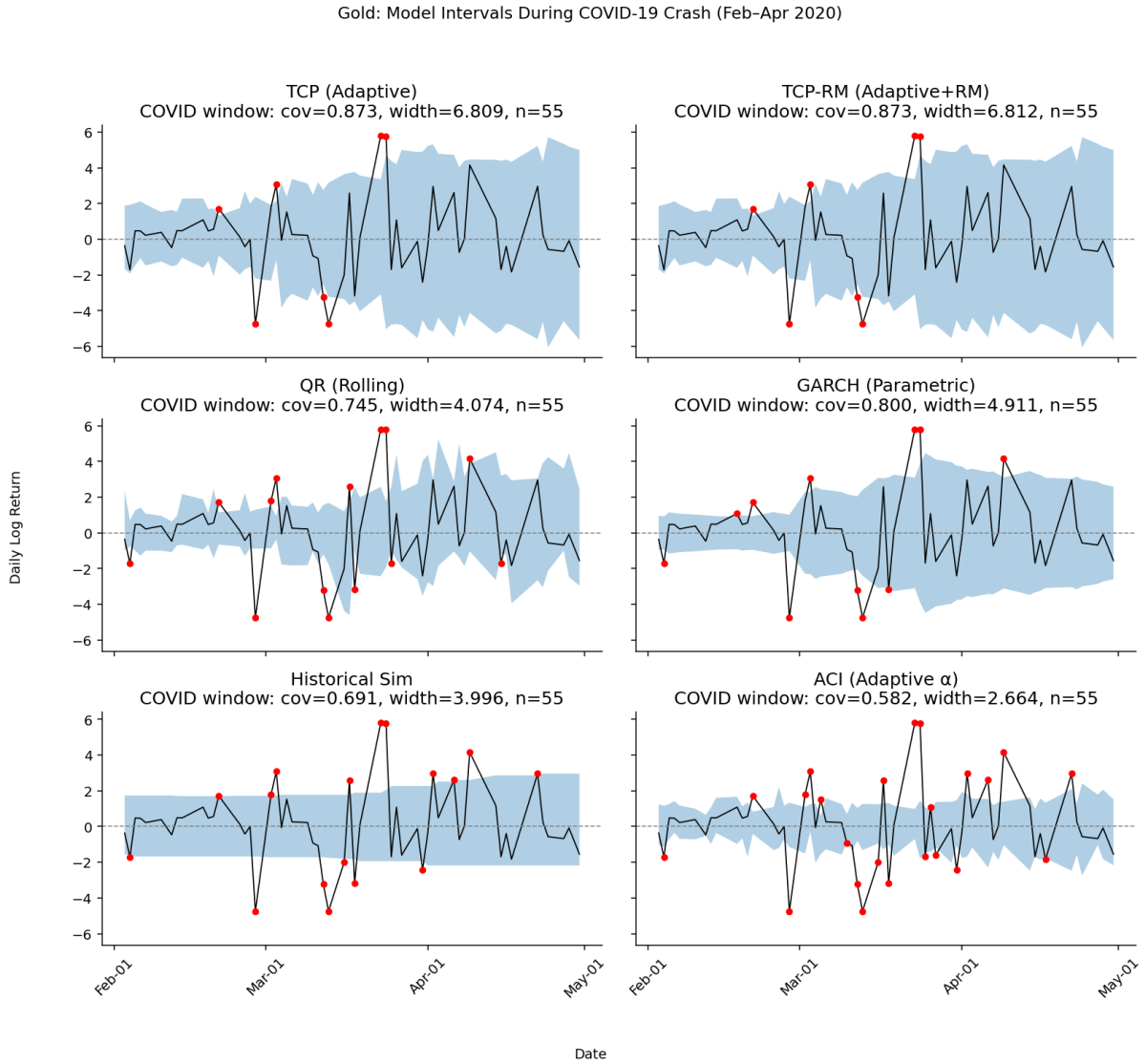


Figure 6: A comparison of 95% prediction intervals from **five** models (TCP, TCP-RM, QR, GARCH, Hist, ACI) for Gold daily returns during the COVID-19 market crash (February-April 2020).

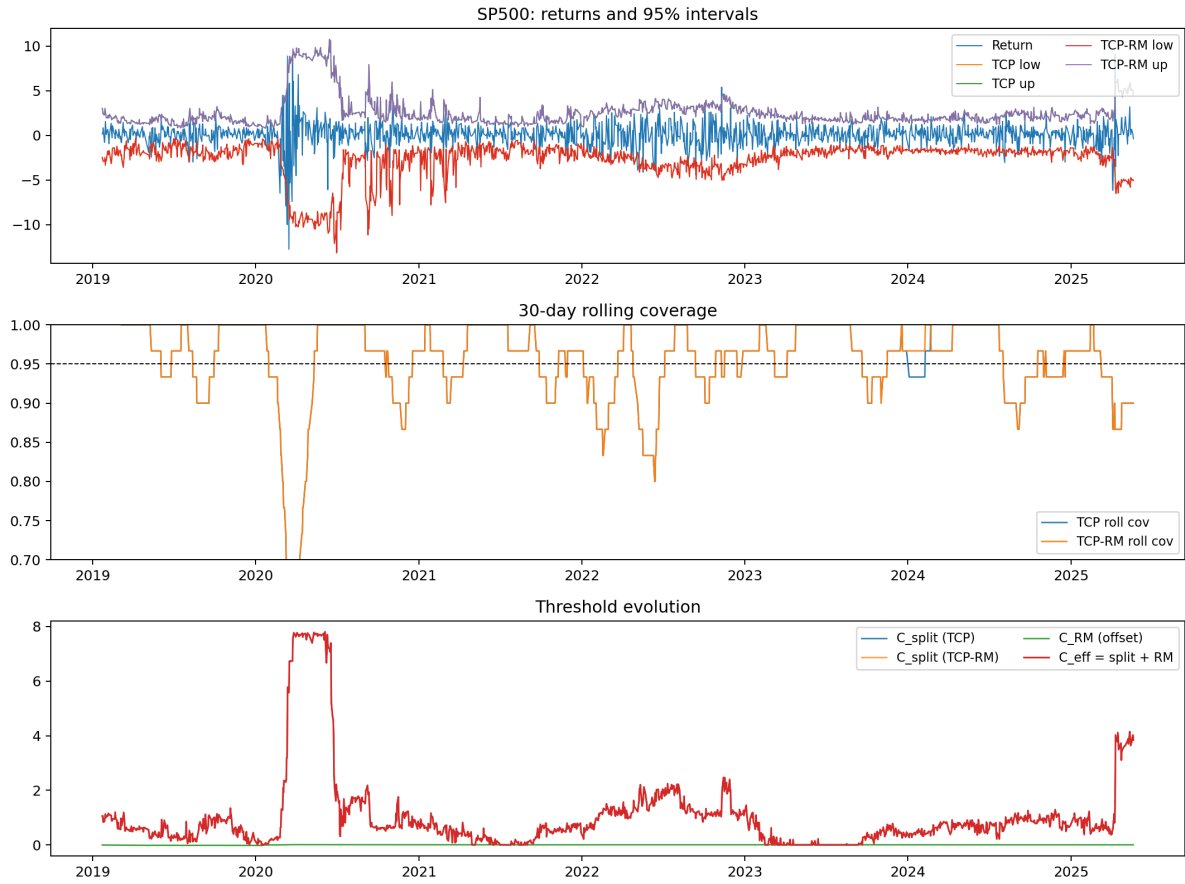


Figure 7: **TCP vs. TCP-RM on S&P 500 (95% intervals)**. Top: daily returns with two-sided prediction bands for TCP (blue) and TCP-RM (purple). Middle: 30-day rolling empirical coverage; the dashed line marks the 95% target. Bottom: evolution of conformal thresholds: split-conformal level  $C_{\text{split}}$ , Robbins–Monro offset  $C_{\text{RM}}$ , and effective total  $C_{\text{eff}} = C_{\text{split}} + C_{\text{RM}}$ . During the COVID-19 crash the bands widen sharply, the rolling coverage briefly moves away from the 95% target and then returns, and  $C_{\text{eff}}$  spikes before decaying as conditions stabilize.

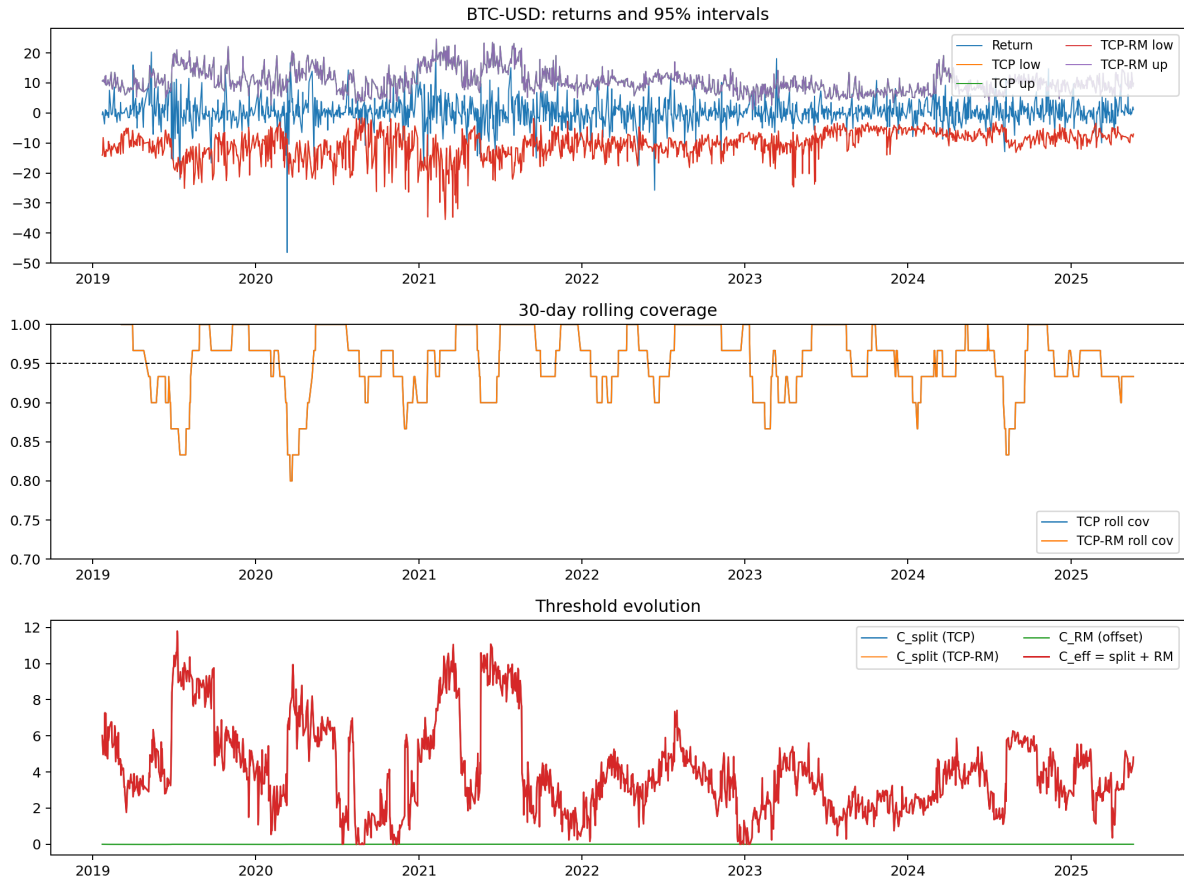


Figure 8: **TCP vs. TCP-RM on BTC-USD (95% intervals)**. Same layout as Figure 7. Large and frequent shocks lead to sustained but controlled elevations in  $C_{eff}$ , which keeps rolling coverage close to 95% while allowing intervals to shrink as volatility recedes.

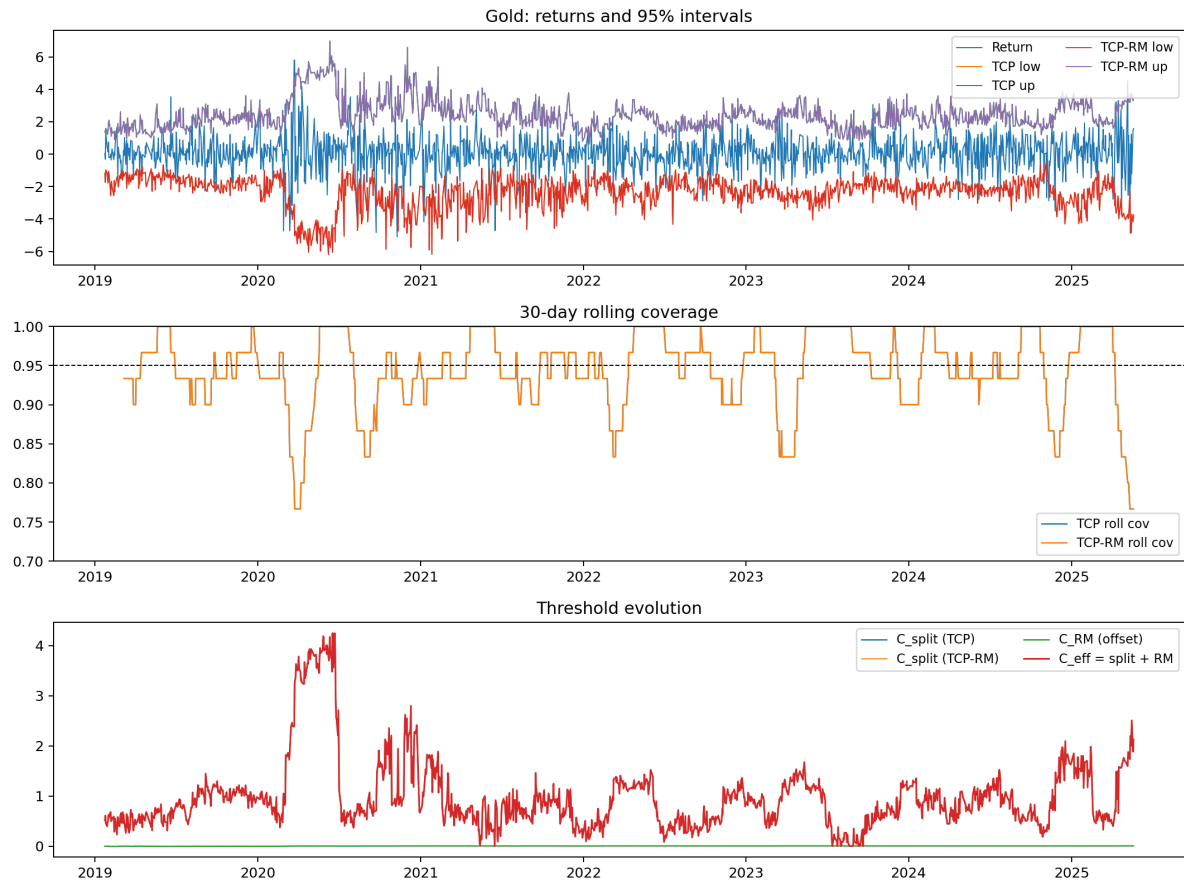


Figure 9: **TCP vs. TCP-RM on Gold (95% intervals)**. Same layout as Figure 7. Spikes in  $C_{\text{eff}}$  are concentrated around crisis windows; away from those periods  $C_{\text{RM}}$  stays close to zero and the method behaves like standard split-conformal TCP.